DENOISING HYPERSPECTRAL IMAGES USING INTERBAND CORRELATION

Shuhei Takehisa and Masahiro Okuda

Doshisha University, Japan

ABSTRACT

This paper proposes a method for self-supervised denoising of hyperspectral images (HSI). Learning-based HSI denoising has limited success because it is often difficult to collect large datasets. To address the difficulty, we proposed a self-supervised approach, in which we exploit the self-similarity that hyperspectral images inherently have among adjacent bands. Unlike other hyperspectral denoising methods based on training a neural network, we do not need any training dataset, and it is possible to restore an image by the CNN trained only by a single noisy input. We demonstrate the validity of our method through some experiments and show that our approach has better or comparable characteristics than conventional methods.

***Index Terms*—** Self-supervised learning, hyperspectral image, image recovery

1. INTRODUCTION

Hyperspectral images (HSI) is useful for a wide range of applications in earth observation, including forest management, precision management, precision agriculture, ecosystem monitoring, resource exploration, and seafloor depth measurement. HSIs are often affected by noise due to their narrow spectral bandwidths, which prevents the precise extraction of useful information in applications such as classification, unmixing, and target detection. To address this issue, various methods have been proposed for denoising HSI. There are image restoration methods that take advantage of the low-rank property, sparsity, and non-local correlation of HSI [1, 2, 3, 4, 5, 6, 7, 8].

Exploiting the self-similarity of images is esssential in some image restoration methods. BM4D ¥citeBM, which is built based on the well-known non-local method BM3D, has been used as a baseline to verify the performances of HSI restoration methods. FastHyDe ¥citeFastHyDe efficiently exploits both the low-rankness and self-similarity. Although these methods realize high performance, they are suitable for Gaussian and Poisson noises. However, CNN-based methods that take into account the self-similarity of HSI have rarely been explored.

In this study, we propose a denoising method using images of adjacent bands. The approach follows the method proposed in [9], where a pair of noisy images is used to produce a clear image. A band in an HSI usually has strong correlations with its adjacent bands, and noises can be modeled as being added to each band independently. Our method takes advantage of this characteristic. The proposed method exploits the self-similarity of HSI and the smoothing property of CNN and can train CNN with only a noisy input image without any other training data.

In the following section, we describe our method based on the noise2noise algorithm [9]. We show the validity of our method through several denoising examples by comparing our method with some conventional HSI denoising methods in Section 3, and then we conclude this work in Section 4.

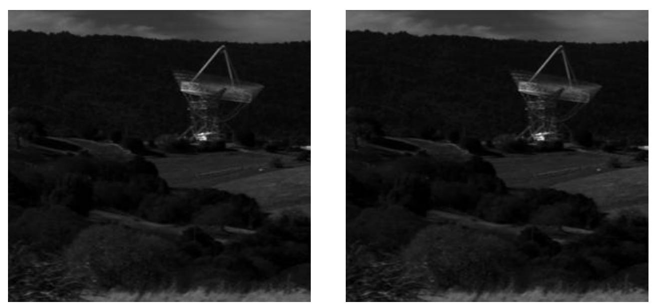

(a) Stanford's 60th band (b) Stanford's 61th band

Fig. 1. Correlations between adjacent bands in HSI: There is high correlations between the adjacent bands (a) and (b).

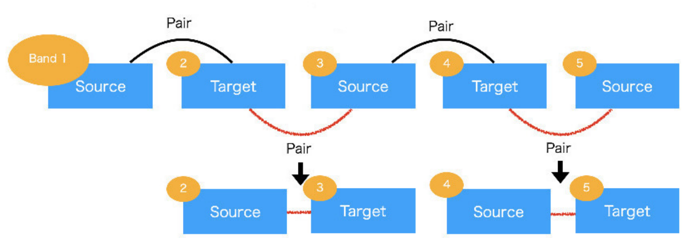

Fig. 2. Image of the data settings for the source and target images. Reusing a band has about twice as many datasets as simply dividing the band into source and target images.

Table 1. Results for Gaussian noise removal (PSNR[dB]/SSIM).

σ	HSI	LRTDTV [10]	SSTV [11]	HSSTV [12]	BM4D [13]	RPCA [14]	our method
0.05	PaviaC	38.29/0.9393	38.02/0.9369	37.32/0.9390	38.53/0.9457	38.25/0.9551	35.58/0.9434
	PaviaU	38.07/0.9418	37.82/0.9381	37.16/0.9417	38.53/0.9481	37.30/0.9531	35.14/0.9431
	Frisco	41.62/0.9634	39.85/0.9449	40.78/0.9667	40.41/0.9603	42.70/0.9813	37.20/0.9440
	Stanford	41.86/0.9676	39.90/0.9394	40.52/0.9634	40.75/0.9630	43.00/0.9785	37.37/0.9510
	WashingtonDC	40.39/0.9586	38.98/0.9285	38.78/0.9464	39.62/0.9511	41.74/0.9717	35.58/0.9702
	AVERAGE	**40.05**/0.9541	38.91/0.9376	38.91/0.9514	39.57/0.9536	40.60/**0.9679**	36.17/0.9503
σ	HSI	LRTDTV	SSTV	HSSTV	BM4D	RPCA	our method
0.15	PaviaC	32.87/0.8515	31.32/0.7544	32.92/0.8393	32.82/0.8565	32.71/0.8620	32.59/0.9004
	PaviaU	32.73/0.8556	31.16/0.7539	32.72/0.8413	32.71/0.8657	30.38/0.8592	31.69/0.8979
	Frisco	36.15/0.9026	31.82/0.7355	34.27/0.8525	34.75/0.8894	35.44/0.9118	34.14/0.8965
	Stanford	35.95/0.9084	32.53/0.7438	34.85/0.8514	35.05/0.8910	35.91/0.9036	32.96/0.8815
	WashingtonDC	35.95/0.8913	32.27/0.7322	34.16/0.8239	33.62/0.8381	34.88/0.8826	33.24/0.9610
	AVERAGE	**34.70**/0.8830	31.82/0.7440	33.78/0.8417	33.79/0.8681	33.78/0.8838	32.92/**0.9074**
σ	HSI	LRTDTV	SSTV	HSSTV	BM4D	RPCA	our method
0.25	PaviaC	28.79/0.7810	25.67/0.4877	27.35/0.5870	30.32/0.7917	29.40/0.7661	30.58/0.8627
	PaviaU	28.62/0.7863	25.51/0.4871	27.17/0.5863	30.01/0.8002	26.93/0.7716	29.96/0.8628
	Frisco	31.72/0.8542	25.87/0.4438	27.85/0.5678	32.32/0.8376	32.18/0.8281	32.41/0.8704
	Stanford	31.75/0.8602	26.64/0.4645	28.62/0.5856	32.66/0.8280	32.67/0.8147	32.00/0.8798
	WashingtonDC	31.70/0.8397	26.46/0.4671	28.30/0.5721	31.20/0.7418	31.99/0.7901	32.84/0.9596
	AVERAGE	30.52/0.8242	26.03/0.4700	27.86/0.5798	31.30/0.7999	30.63/0.7941	**31.56/0.8871**

2. SELF-SUPERVISED LEARNING FOR HSI DENOISING

The proposed method takes advantage of the feature that an HSI has high self-similarity among bands. The adjacent bands of an HSI are shown in Figure 1. These figures show some neighboring bands of the *Stanford* and *Indian*. One can see that the adjacent bands are similar when a spectral interval is small. We use this self-similarity to restore HSIs.

Lehtinen et al. [9] introduce a method to restore latent images using a high correlation between two measurements on a noisy image pair. The technique exploits the implicit smoothing properties of CNNs, and they experimentally proved that a training set of clear images is not necessary as supervised data to learn a denoising network. Our work is inspired by this technique.

We consider a simple additive degradation model:

$$y = x + n \tag{1}$$

where n denotes additive noises. We consider Gaussian noise with standard deviation σ and/or line noises in our experiments. Our goal is to estimate the latent clear image x from the degraded observation y. In our method, we train a CNN model with pairs (y_i, y_{i+1}) consisting of two noisy adjacent bands in an HSI, where subscript i indicate the indices of the bands. One of the images is used as the source image and the other as the target image for training. We create a dataset by slicing the HSI data and convert it to a set of 2D images. Next, every pair of two adjacent images is set as source and target images. The image diagram is shown in Figure 2.

We train a neural network by minimizing the following equation with the supervised image pair $\hat{x_i} = y_i$ and a target y_{i+1}:

$$\arg\min_{\theta} \sum_i L(f_\theta(\hat{x_i}), y_i) \tag{2}$$

where f_θ is the neural network.

In this experiment, the loss function is based on L2 loss, and the learning is done using U-net. The parameters of this network are the same as in Lehtinen et al[9]. In our method,

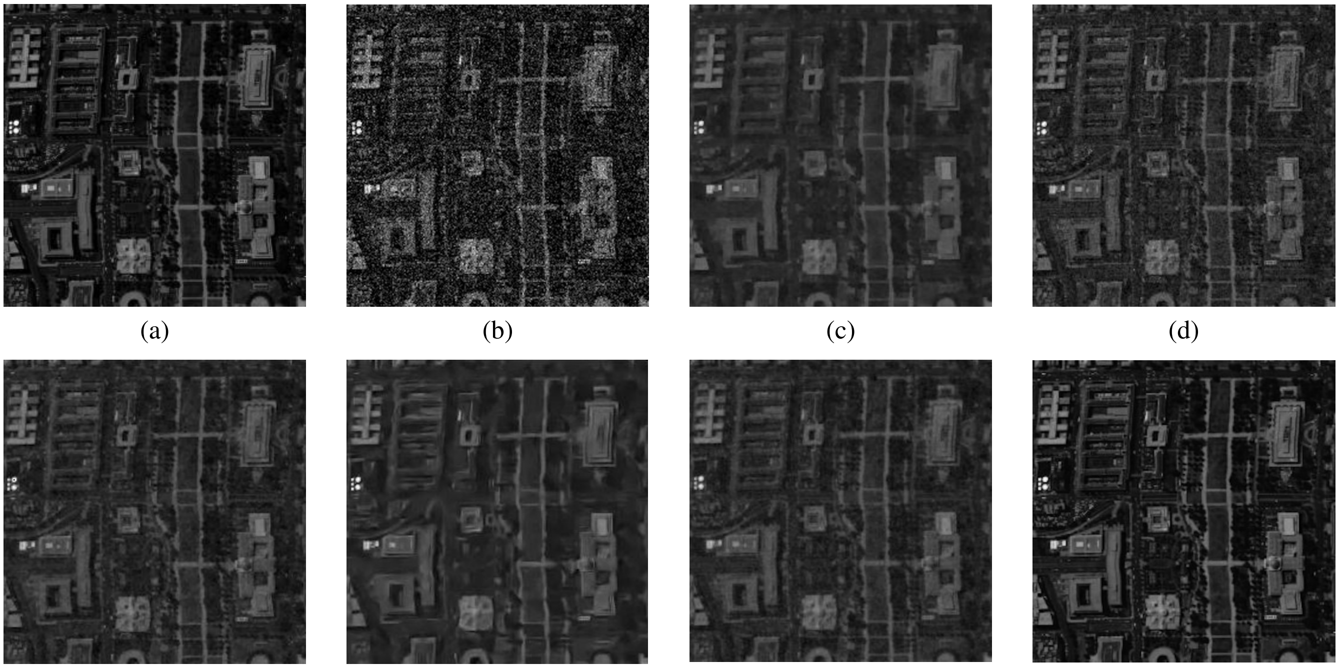

(a) (b) (c) (d)

(e) (f) (g) (h)

Fig. 3. Experimental results of removing Gaussian noise of WashingtonDC (30th band). (a)original image, (b)observation, (c)LRTDTV, (d)SSTV, (e)HSSTV, (f)BM4D, (g)RPCA, (h)our method

we train a network by a single HSI to be denoised. Training was done using ADAM with parameter values ($\beta_1 = 0.9, \beta_2 = 0.99, \epsilon = 10^{-8}$).

3. EXPERIMENT

We evaluated our experimental results with PSNR and SSIM. In order to evaluate the validity of our method, we compare our method with LRTDTV [10], SSTV [11], HSSTV [12], BM4D [13] and RPCA [14]. The standard deviation σ of Gaussian noise is set to σ = 0.05, 0.15, 0.25. The HSI to be compared is commonly used in the HSI community. These are the five HSIs, *Stanford, PaviaC, PaviaU, Frisco, and WashingtonDC*. We add two types of noises to these images, Gaussian noise only and Gaussian noise and line noises.

The experimental results are shown in Tables 1 and 2. Table 1 shows the results for Gaussian noise, and Table 2 shows the results for Gaussian noise + line noise. PSNR values and SSIM values indicate the mean of PSNR and SSIM for all bands. The bold numbers indicate the best performance. Fig.3 and Fig.4 show the actual denoised identical images processed by the methods. Compared to the other methods, our method is less accurate when the noise intensity is low, although it outperformes the others when it is high. In particular, it has the highest accuracy in the evaluation of SSIM. Fig.3 shows that Gaussian noise is successfully reduced by all the methods, while there are some differences in clarity. In (d), (e), and (f), the line noise remains, while it is successfully removed in (c), (g), and (h).

4. CONCLUDING REMARKS

In this paper, we proposed a denoising method for HSI. The denoising method is based on the fact that HSI is composed of highly correlated images. Since exploiting pairs of the same bands with different noise on them enables denoising, it is possible to remove the additive noise with our self-supervised manner. Our method uses self-supervised learning and can perform as well or better than other superior denoising methods. Moreover, our method requires for the training only one image to be denoised. Thus it is possible to operate at a low cost. HSI essentially costs a lot to capture, and it is thus one of the critical points that the cost for denoising is low. Therefore, we expect it to be an effective tool for denoising HSI.

5. REFERENCES

[1] H. K. Aggarwal and A. Majumdar., "Hyperspectral image denoising using spatio-spectral total variation.," *IEEE Geosci. Remote Sens. Lett.*, 13(3):442—446, 2016.

[2] W. He, H. Zhang, L. Zhang, and H. Shen., "Total-variationregularized low-rank matrix factorization for

Table 2. Results for Gaussian + line noise removal (PSNR[dB]/SSIM).

σ	HSI	LRTDTV [10]	SSTV [11]	HSSTV [12]	BM4D [13]	RPCA [14]	our method
0.05	PaviaC	37.66/0.9386	30.37/0.8982	30.26/0.9003	29.72/0.9021	38.23/0.9482	34.52/0.9376
	PaviaU	37.35/0.9408	31.01/0.9046	30.83/0.9081	30.39/0.9109	37.26/0.9385	33.73/0.9378
	Frisco	40.78/0.9627	31.18/0.8983	31.28/0.9207	29.95/0.9079	42.69/0.9767	35.46/0.9412
	Stanford	41.22/0.9671	34.01/0.9112	34.27/0.9382	32.04/0.9297	42.97/0.9750	36.05/0.9442
	WashingtonDC	39.63/0.9575	32.16/0.8962	32.31/0.9164	31.47/0.9163	41.72/0.9692	33.79/0.9712
	AVERAGE	39.33/0.9533	31.75/0.9017	31.79/0.9167	30.71/0.9134	**40.57**/**0.9615**	34.71/0.9464
σ	HSI	LRTDTV	SSTV	HSSTV	BM4D	RPCA	our method
0.15	PaviaC	32.73/0.8506	28.47/0.7396	29.17/0.8235	28.46/0.8181	32.30/0.8297	31.63/0.8863
	PaviaU	32.38/0.8572	28.77/0.7420	29.54/0.8310	28.88/0.8314	30.35/0.7437	30.95/0.8879
	Frisco	35.39/0.9043	29.00/0.7193	30.15/0.8396	29.90/0.8444	35.40/0.8954	32.57/0.8905
	Stanford	35.55/0.9082	30.95/0.7406	32.50/0.8539	31.53/0.8667	35.89/0.8890	33.43/0.8935
	WashingtonDC	34.50/0.8915	29.89/0.7232	30.96/0.8192	29.93/0.8106	34.84/0.8741	34.04/0.9725
	AVERAGE	**34.11**/0.8824	29.42/0.7329	30.46/0.8334	29.58/0.8342	33.76/0.8464	32.52/**0.9061**
σ	HSI	LRTDTV	SSTV	HSSTV	BM4D	RPCA	our method
0.25	PaviaC	30.42/0.7808	26.12/0.5666	27.74/0.7224	27.52/0.7598	29.38/0.7135	29.23/0.8114
	PaviaU	30.09/0.7845	26.19/0.5665	27.91/0.7275	27.68/0.7708	26.90/0.5705	29.57/0.8524
	Frisco	33.01/0.8537	26.52/0.5336	28.64/0.7345	28.41/0.7965	32.14/0.8028	31.57/0.8761
	Stanford	33.40/0.8585	27.95/0.5619	30.51/0.7554	30.54/0.8118	32.67/0.7929	32.34/0.8766
	WashingtonDC	32.12/0.8381	27.31/0.5520	29.32/0.7153	28.91/0.7209	31.94/0.7851	33.59/0.9688
	AVERAGE	**31.83**/0.8231	26.82/0.5561	28.82/0.7310	28.61/0.7720	30.61/0.7330	31.26/**0.8771**

hyperspectral image restoration.," *IEEE Trans. Geosci. Remote Sens.*, 54(1):178—188, 2016.

[3] Y. Wang, J. Peng, Q. Zhao, Y. Leung, X.-L. Zhao, and D. Meng., "Hyperspectral image restoration via total variation regularized low-rank tensor decomposition.," *IEEE Journal of Selected Topics in Applied Earth Observations and Remote Sensing*, 11(4):1227—1243, 2018.

[4] Q. Yuan, L. Zhang, and H. Shen., "Hyperspectral image denoising employing a spectral-spatial adaptive total variation model.," *IEEE Trans. Geosci. Remote Sens.*, 50(10):3660—3677, 2012.

[5] H. Zhang, W. He, L. Zhang, H. Shen, and Q. Yuan, "Hyperspectral image restoration using low-rank matrix recovery.," *IEEE Trans. Geosci. Remote Sens.*, 52(8):4729—4743, 2014.

[6] Ryota Yuzuriha, Ryuji Kurihara, Ryo Matsuoka, and Masahiro Okuda, "Tnng: Total nuclear norms of gradients for hyperspectral image prior," *Remote Sensing*, vol. 13, no. 4, pp. 819, 2021.

[7] Ryuji Imamura, Tatsuki Itasaka, and Masahiro Okuda, "Zero-shot hyperspectral image denoising with separable image prior," in *Proceedings of the IEEE/CVF International Conference on Computer Vision Workshops*, 2019, pp. 0–0.

[8] Mia Rizkinia and Masahiro Okuda, "Joint local abundance sparse unmixing for hyperspectral images," *Remote Sensing*, vol. 9, no. 12, pp. 1224, 2017.

[9] J.Lehtinen, J.Munkberg, J.Hasselgren, S.Laine, T.Karras, M.Aittala, and T.Aila, "Noise2noise: Learning image restoration without clean data," *International Conference on Machine Learning(ICML)*, March 2018.

[10] Wang Y., Peng J., Zhao Q., Leung Y., Zhao X.L., and D Meng, "Hyperspectral image restoration via total variation regularized low-rank tensor decomposition.,"

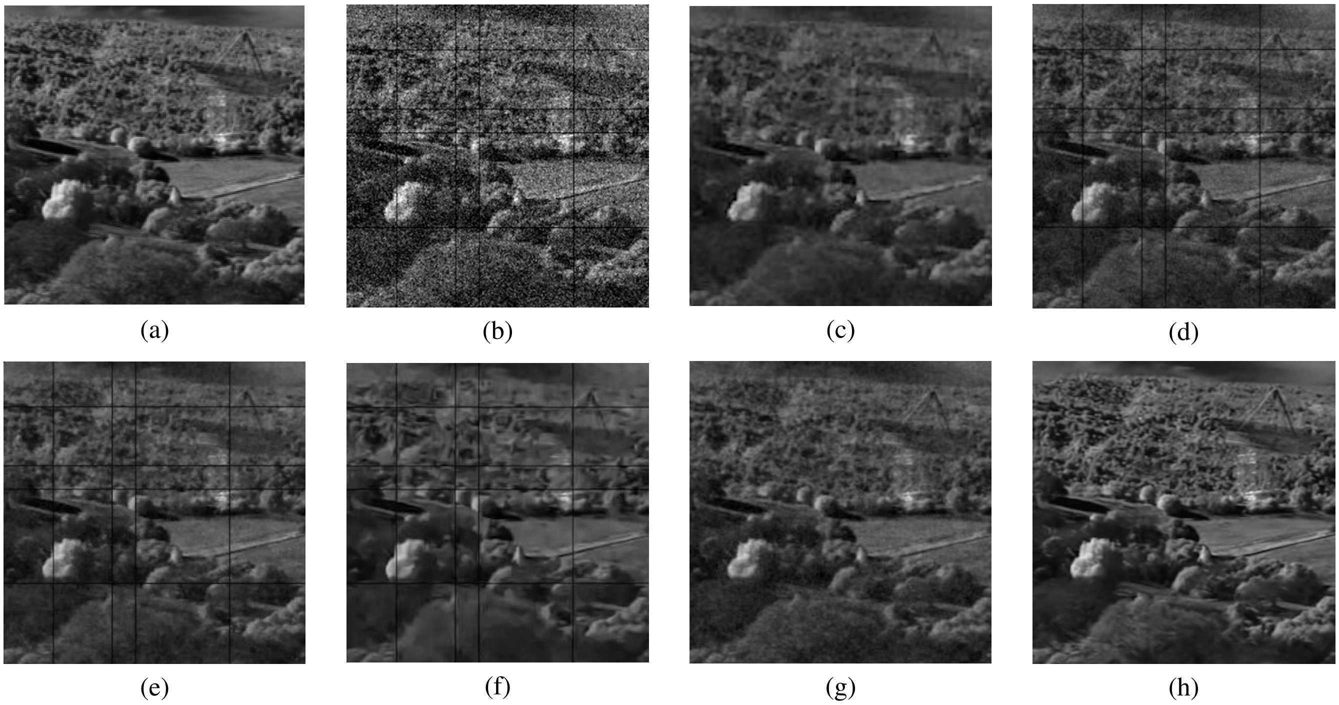

Fig. 4. Experimental results of removing Gaussian noise and line noise of Stanford (130th band). (a)original image, (b)observation, (c)LRTDTV, (d)SSTV, (e)HSSTV, (f)BM4D, (g)RPCA, (h)our method

IEEE J. Sel. Top. Appl. Earth Obs. Remote Sens., 11, pp. 1227–1243, 2018.

[11] Aggarwal H.K. and Majumdar A., "Hyperspectral image denoising using spatio-spectral total variation.," *IEEE Geosci. Remote Sens.Lett., 13*, p. 442–446, 2016.

[12] Takeyama S., Ono S., and Kumazawa I., "Hyperspectral image restoration by hybrid spatio-spectral total variation.," *In Proceedings of the 2017 IEEE International Conference on Acoustics, Speech and Signal Processing, New Orleans, LA, USA*, pp. 4586–4590, March 2017.

[13] M. Maggioni, K. Egiazarian, and A. Foi., "Nonlocal transform-domain filter for volumetric data denoising and reconstruction.," *IEEE Trans. Image Process.*, pp. 119–133, 2013.

[14] E.J. Candès, X. Li, Y. Ma, and J. Wright., "Robust principal component analysis?," *ACM 58*, p. 37, May 2011.